Role of free-carrier interaction in strong-field excitations in semiconductors

Richard Hollinger,[1,2,*] Elissa Haddad,[3] Maximilian Zapf,[4] Valentina Shumakova,[5] Paul Herrmann,[1] Robert Röder,[4] Ingo Uschmann,[1,2] Udo Reislöhner,[4] Audrius Pugžlys,[5] Andrius Baltuška,[5] Francois Légaré,[3] Michael Zürch,[1,6,7,8] Carsten Ronning,[4,9] Christian Spielmann,[1,2,9] and Daniil Kartashov[1,9]

[1]*Institute of Optics and Quantum Electronics, Friedrich-Schiller-University Jena, Max-Wien-Platz 1, 07743 Jena, Germany*
[2]*Helmholtz Institute Jena, Fröbelstieg 3, 07743 Jena, Germany*
[3]*Centre Énergie Matériaux et Télécommunications, Institut National de la Recherche Scientifique, 1650 Boulevard Lionel-Boulet, Varennes, Québec, Canada J3X1S2*
[4]*Institute for Solid State Physics, Friedrich-Schiller-University Jena, Max-Wien-Platz 1, 07743 Jena, Germany*
[5]*Institute for Photonics, Technical University Vienna, Gußhausstrasse 25-29, 1040 Vienna, Austria*
[6]*Fritz Haber Institute, Faradayway 4-6, 14195 Berlin, Germany*
[7]*Department of Chemistry, University of California Berkeley, 237B Hildebrand Hall, Berkeley, California 94720, USA*
[8]*Lawrence Berkeley National Laboratory, Materials Sciences Division, Berkeley, California 94720, USA*
[9]*Abbe Center of Photonics, Friedrich Schiller University, Jena, Albert Einstein Straße 6, 07745 Jena, Germany*

(Received 22 February 2021; accepted 24 June 2021; published 15 July 2021)

The interaction of laser pulses with condensed matter forms the basis of light-wave-driven electronics potentially enabling tera- and petahertz switching rate applications. Carrier control using near- and midinfrared pulses is appealing for integration into existing platforms. Toward this end, a fundamental understanding of the complexity of phenomena concerning sub-band-gap driven semiconductors such as high harmonic generation, carrier excitation due to multiphoton absorption, and interband tunneling as well as carrier-carrier interactions due to strong acceleration in infrared transients is important. Here, stimulated emission from polycrystalline ZnO thin films for pump wavelengths between 1.2 μm (1 eV) and 10 μm (0.12 eV) is observed. Contrary to the expected higher intensity threshold for longer wavelengths, the lowest threshold pump intensity for stimulated emission is obtained for the longest pump wavelength corroborating the importance of collisional excitation upon intraband electron acceleration.

DOI: 10.1103/PhysRevB.104.035203

I. INTRODUCTION

Nowadays, transistor technology is one of the main drivers of modern electronics, and the computational power of integrated circuits (ICs) is defined by the number of transistors. Due to the continuous minimization of ICs to increase the number of transistors on chips, the current flow leads to a high level of dissipative energy, which, together with quantum uncertainties of the electronic states, led to stagnation in the number of transistors on chips [1]. A further increase of the electronic switching rate and thus computational power therefore requires new approaches. To investigate electron processes beyond the current GHz limit of electronics, controlled light waveforms (ultrashort laser pulses) provide a powerful tool to push the frontiers of electronics. Ultrashort laser pulses in the visible to the near-infrared spectral range with tera- and petahertz carrier waves have already shown great promise to investigate new switching methods that can overcome the limits of conventional transistor-based electronics [2–6]. Under the interaction with intense light fields, quasifree electrons are controlled in semiconductors and dielectrics at every half-cycle of the laser pulse electric field, thus inducing a periodic material modification. These quasifree electrons can gain a significant amount of kinetic energy from the electric fields of intense laser pulses leading to a coherent current, which can be measured using metallic-dielectric nanojunctions [7] or in the form of high harmonic orders of the fundamental laser pulse spectrum [8].

High harmonic generation (HHG) from a near to mid-infrared (mid-IR) laser in solids originates from a highly nonlinear intraband current and interband recombination upon photoexcitation and acceleration of the electrons by the strong laser field [see Figs. 1(a) and 1(b)] [9,10]. Since carrier injection and current generation are periodically repeated every half-cycle of the laser pulse electric field, HHG presents an ultrafast electronic metrology of tera- and petahertz switching processes in solids [11,12]. If the energy transfer from the laser field to the free electrons in the conduction band (CB) is larger than the material band gap, the highly energetic free electron in the CB can excite a bound electron from the valence band (VB) via electron collisional excitation [Fig. 1(c)]. The average kinetic energy of free electrons in oscillating electric fields (ponderomotive energy, U_p) scales linearly with the laser intensity and quadratically with the wavelength ($U_p \sim I\,\lambda^2$) [13]. In solids, this simple scaling holds as well within the parabolic band approximation, i.e., in the vicinity of the Γ-point. In general, an electron's energy is defined by its position in the band, and therefore it scales linearly with the field strength and with the wavelength following the

*Corresponding author: richard.hollinger@uni-jena.de

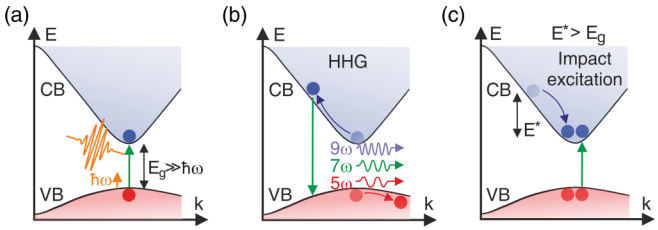

FIG. 1. Inter- and intraband processes in strong-field excited semiconductors. (a) Interband excitation of an electron (blue sphere) by creating a valence-band hole (red sphere) upon far-off-resonance absorption of light with a photon energy $\hbar\omega$ much smaller than the material band gap E_g via a multiphoton and tunneling process. (b) High harmonic generation (HHG) in solids. After field excitation, the quasifree electron is driven by the strong electric field of the laser pulse. The electron displacement leads to a nonlinear intraband current, together with an interband polarization field upon an electron-hole recombination process, which results in the generation of high harmonic orders of the fundamental driving field. (c) If the electron gains sufficient energy such that the kinetic energy exceeds the band-gap energy, the highly energetic electron in the CB can transfer its energy to a VB electron via electron-electron interaction. As a result, a VB electron is excited to the CB.

solution for quasimomentum. Thus, intense long-wavelength light can be applied to very efficiently multiply the number of excited carriers in a controlled manner [14], or it can trigger an avalanche excitation process [15]. Furthermore, using long-wavelength light in the telecom wavelength range (1.2–1.6 μm) for light-based tera- to petahertz electronic applications is beneficial for the integration in existing platforms [16]. Therefore, detailed knowledge of the electron response upon intense long-wavelength light interaction in the near- to midinfrared spectral range is of crucial importance for future technological progress.

It was recently demonstrated that dynamically and coherently driven carriers can significantly contribute to interband carrier injection in ultrafast pump-probe experiments [17,18], in agreement with theoretical simulations [19,20]. Furthermore, electron excitation processes in dielectrics and semiconductors upon strong light field-matter interaction were studied by investigating the laser-induced damage threshold [15] or plasma formation threshold [21].

The onset of optically pumped lasing, i.e., when the gain due to stimulated emission is sufficient to overcome all losses, can be used to monitor the excited electron density upon the absorption of the pump light. It was already shown that the gain provided by the semiconductor material only depends on the density of excited electrons [22]. Polycrystalline ZnO thin films on sapphire substrates are a well-known morphology supporting lasing in the near-ultraviolet (NUV) spectral range [23]. Optically pumped lasing from ZnO films upon photoexcitation via a single- and up to five-photon absorption process was demonstrated previously [23–25]. The possibility to achieve population inversion in ZnO upon optical excitation using off-resonant light, even in the tunneling excitation regime, has been demonstrated recently in ZnO bulk and nanowire samples [26,27].

Here, the onset of far-off-resonance pumped lasing is systematically studied in polycrystalline ZnO thin films. Stimulated emission is confirmed by spectral as well as time-domain measurements depending on the excitation intensity far off the material resonance using a 3.2 μm laser for pumping. Criteria for the onset of lasing are defined from the experimentally easily accessible emission spectra. To investigate light absorption in ZnO, the onset of lasing was determined for pump wavelengths in the wide spectral range where the band-gap to photon-energy ratios are in the range between 4 and 26. The measured material response as a function of the laser wavelength is in very good agreement with simulations, which include multiphoton and tunneling excitation as well as collisional excitation upon free-carrier absorption.

II. METHODS

Intrinsic, approximately 300-nm-thick polycrystalline ZnO thin films were grown by magnetron rf-sputtering (rf-power about 150 W) on 0.5-mm-thick *c*-plane sapphire substrates at a pressure of about 2.95×10^{-3} mbar in an argon atmosphere with a small amount (2 vol. %) of oxygen. Subsequently, the samples were thermally annealed in air at 900 °C for 60 min. The structural properties of the films were analyzed using scanning electron microscopy (SEM) and x-ray diffraction (XRD) techniques (see the Supplemental Material [28] for more details).

Optical excitation of the films in the wavelength range from 1.2 up to 2.5 μm for the signal and idler output of a two-stage optical parametric amplifier (OPA) was used. The OPA was pumped by 5 mJ, 35 fs pulses centered at 800 nm, at a repetition rate of 1 kHz. The midinfrared (mid-IR) pulses between 3 and 4 μm wavelength were generated by noncollinear difference frequency generation (DFG) between the signal and idler waves from the OPA in a potassium titanyl arsenate (KTA) crystal. Laser pulses with a longer wavelength at 10 μm were generated by collinear DFG in a gallium selenide (GaSe) crystal between the signal and idler of a three-stage OPA, initially pumped with 1.1 mJ pulses at 800 nm, with a 50 Hz repetition rate and 35 fs duration. The pulse durations were experimentally determined using frequency resolved optical gating (FROG), intensity autocorrelation, and discrete D-Scan techniques [40]. The focal spot at every wavelength was experimentally measured using the knife-edge technique. The laser intensity was calculated from the pulse duration, energy, and the focal spot size. The femtosecond mid-IR laser pulses were focused onto the ZnO thin films using an $f = 10$ cm CaF_2 lens and an $f = 7.5$ cm gold-coated concave mirror (see the Supplemental Material [28]) in the case of a 1.2–4 μm and a 10 μm pump wavelength, respectively. Wire grid polarizers were used to adjust the laser power exciting the thin film sample. In the experiment, the laser beam was focused at the film deposited side of the substrate. The NUV emission from the ZnO thin film was collected and collimated with a lens on the blank side of the sapphire substrate and refocused onto the entrance slit of a spectrometer (Ocean Optics USB4000). The temporal dynamics of the emission was measured using an up-conversion method [41]. Therefore, the NUV emission was overlapped with a time delayed 60-fs-long laser pulse centered at 0.8 μm in a type II BBO ($\vartheta = 55°$) to generate the sum frequency (SFG). The SFG signal was detected using a photomultiplier in combination with a lock-in amplifier

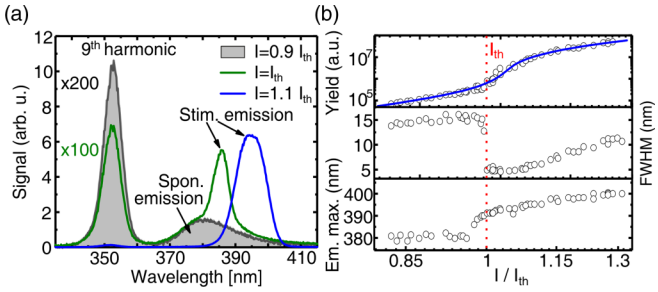

FIG. 2. Lasing in polycrystalline ZnO thin films pumped in the tunneling excitation regime using laser pulses at 3.2 μm wavelength. (a) Spectral evolution of the near ultraviolet (NUV) emission as a function of the pump laser intensity. The transition between a regime below the lasing threshold I_{th} where the spectra are dominated by high harmonic and spontaneous emission (gray area) to largely stimulated emission above the lasing threshold is evident by a strong lasing peak appearing around 395 nm (blue). (b) Integrated emission yield, full width at half maximum (FWHM), and wavelength of the emission maximum as a function of the pump laser intensity. The blue line depicts the calculated values using the rate equation model, and the red dotted line marks the threshold intensity. See the text for details.

(see the Supplemental Material [28]). All experiments were performed at room temperature and ambient conditions.

III. RESULTS AND DISCUSSION

A. Far-off-resonance optically pumped lasing in polycrystalline ZnO thin films

First, polycrystalline ZnO thin films were pumped far-off-resonance by femtosecond laser pulses at 3.2 μm, which corresponds to a band-gap to photon-energy ratio of 9. Figure 2(a) shows the measured emission spectra of a ZnO thin film for three different pump laser intensities—below, around, and above the lasing threshold. For low pump laser intensities (gray area), two distinct peaks at 355 nm and around 380 nm are visible. The peak at 380 nm originates from the spontaneous emission due to the recombination of free excitons [23,42], and the peak at 355 nm corresponds to the ninth-order harmonic of the 3.2 μm pump laser. In these experiments, higher-order harmonics were detected up to the limit defined by experimental constraints [43] (see the Supplemental Material [28] for more details). When increasing the pump power to the lasing threshold (green curve), a new narrow emission band evolves around 385 nm. This peak is rapidly growing, broadening, and redshifting with increasing pump laser intensity and originates from stimulated recombination in an electron-hole plasma (EHP) [23,42]. At the highest pump intensities (blue curve), the stimulated emission peak originally at 385 nm redshifts up to 400 nm due to band-gap renormalization, and its signal intensity dominates the measured spectrum. At such high pump intensities, the contributions by spontaneous emission from free excitons and the high harmonic generation become negligible in comparison to the stimulated emission of ZnO.

Further insight into the dependence of the NUV-emission spectra on the laser intensity is depicted in Fig. 2(b). It shows the output yield given by the spectrally integrated signal (upper panel) as well as the full width at half-maximum (FWHM) (middle panel), and the spectral redshift (lower panel) for the peaks resulting from spontaneous free-exciton emission (below the threshold) and stimulated emission in an EHP (above the threshold) as a function of the pump laser intensity. The red dashed line indicates the pump threshold intensity $I_{th} = 0.275$ TW/cm^2 when stimulated emission starts dominating the emission spectra. For pump intensities below the threshold, the yield follows a linear trend in the log-log representation. When the threshold intensity is reached, the emission yield increases nonlinearly. Calculations using the rate equations [see Eqs. (1)–(3) in the Supplemental Material [28]] reproduce the lasing emission as a function of the laser intensity with high fidelity, as depicted by the blue line in the upper panel of Fig. 2(b), enabling us to extract the threshold intensity. Note that the pump threshold intensity I_{th} reveals a strong pump laser spot size dependence, i.e., threshold intensity increases with reduced excitation spot size (for more details, see the Supplemental Material [28]). This allows us to attribute the detected stimulated emission to both amplified spontaneous emission (ASE) and a random lasing mechanism [31,33]. The linewidth from an EHP-based stimulated emission shows a much narrower FWHM (5–7 nm) compared to a width of 15–17 nm for the free-exciton emission spectra. Increasing the laser intensity further above the threshold value leads to a broadening of the stimulated emission spectra from 5 to 12 nm linewidth, as depicted in the middle panel of Fig. 2(b). This observation can be explained by the broadening of the gain spectra due to an increasing carrier density and heating of the material [22,44–46]. The spectral position of the emission peak maximum is constant below the threshold intensity value as shown in the lower panel of Fig. 2(b). This is indeed indicative of an exciton-based emission process [47]. When increasing the pump intensity values above the threshold, the stimulated emission peak shifts from 390 to 400 nm (redshift) due to band-gap renormalization in the EHP excited in ZnO [22].

From the spectrally resolved measurements, the onset of lasing was linked to the abrupt increase of the emission yield and narrowing of the linewidth, respectively. To further confirm that these spectral features correspond to the lasing threshold and thus the material inversion, time- and polarization-resolved measurements of the NUV emission were performed. Analyzing the polarization state of the emission revealed that the spontaneous emission at 380 nm was not polarized while the stimulated emission at 390 nm emission was clearly polarized, which is another indicator of ASE and random lasing (see the Supplemental Material [28]).

Using nonlinear frequency mixing of the NUV emission and a near-infrared gate pulse, the temporal emission dynamics for three different pump intensities were measured (Fig. 3). The up-converted high harmonic signal was used to calibrate the zero time delay. For excitation intensities below the lasing threshold I_{th} (gray area), only a slow decaying signal was measured, which is attributed to the spontaneous decay of carriers in ZnO [44,48]. At the lasing threshold intensity (green curve), a fast decaying signal appears superimposed to the slower spontaneous emission. With increasing pump intensity, this fast decaying signal is rapidly growing and its

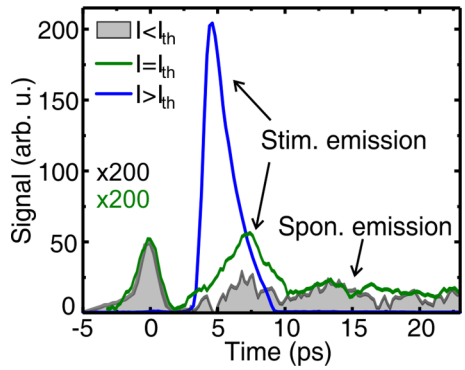

FIG. 3. Temporally resolved NUV emission from ZnO thin films after strong off-resonance excitation using laser pulses at 3.2 μm.

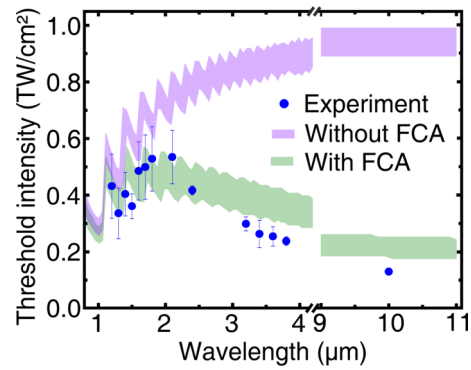

FIG. 4. Pump laser threshold intensities for lasing in a ZnO thin film as a function of the pump laser wavelength (measurements, blue dots). The green and purple parameter margin bands depict the simulated intensity with and without including free-carrier absorption (FCA), respectively, which has to be applied to excite 1×10^{19} cm^{-3} electrons and correspondingly to the provision of gain in the ZnO. See the text for details.

onset appears earlier (blue curve). Due to its short duration of 2–3 ps (FWHM), this signal is attributed to the stimulated emission process in ZnO [49]. The change from a slow to a fast decaying dynamics occurs at the threshold for stimulated emission, as determined by analyzing the power dependence of the spectral emission yield and width (see Fig. 2). In combination, the results of spectrally and temporally as well as polarization-resolved measurements (see the Supplemental Material [28]) indicate that laser emission from polycrystalline ZnO thin films is governed by optical excitation with far-off-resonance 3.2 μm laser pulses.

Creating population inversion in the material and enabling negative absorption, i.e., achieving optical gain in ZnO, requires a threshold carrier density of at least $\sim 1 \times 10^{19}$ cm^{-3} in the conduction band [22,44]. This threshold carrier density represents a universal quantitative parameter for ZnO as an active laser medium, which is independent of the geometry or structure [22]. Furthermore, it was shown that the emission process is temporally decoupled from light absorption by the carrier thermalization process [50]. Indeed, the characteristics of the spectral evolution of the ZnO emission are identical and independent of the pump wavelength in a wide spectral range from 1.2 to 10 μm (see the Supplemental Material [28]). This allows us to use the experimentally observable lasing threshold in ZnO to study the excitation of carriers by far-off-resonance intense laser light.

B. Wavelength scaling of pump threshold intensity

The ZnO thin film was optically pumped at several wavelengths ranging from 1.2 to 10 μm. This corresponds to a band-gap to photon-energy ratio of 4 and up to 26. The pump laser spot size was fixed to a radius of 175 ± 10 μm and the pulse duration was kept in the range of 110 ± 30 fs to assure comparable experimental conditions.

Figure 4 shows the wavelength dependence of the threshold pump intensity for lasing emission. The blue dots correspond to the experimental results. When increasing the pump wavelength from 1.2 to 2 μm, the threshold pump intensity increases from 0.3 to 0.55 TW/cm^2. Further increasing the wavelength leads to a continuous decrease of the lasing threshold. While for pump wavelengths between 3 and 4 μm the determined laser intensity was between 0.3 and 0.2 TW/cm^2, it was only 0.13 TW/cm^2 for a pump wavelength of 10 μm in the far-IR. A deeper understanding of the observed wavelength scaling of the lasing threshold and thus the wavelength-dependent absorption in ZnO is gained by simulations performed using the coupled system of rate equations (see the Supplemental Material [28]).

The excitation process occurs via interband transitions as a result of multiphoton absorption and electron tunneling excitation (see the Supplemental Material [28]) as well as impact ionization upon free-carrier absorption (FCA). The photoemission is temporally decoupled from the excitation process due to hot carrier thermalization. Since the carrier thermalization on a picosecond timescale is much longer than the femtosecond laser pulse duration [50], only the excitation part [Eq. (1) in the Supplemental Material [28]] of the rate equation system was considered to estimate the excited electron density as a function of the laser wavelength and intensity. Thereby, the interband electron generation rate is described by the Keldysh formula [42], and the Drude-like model is used to model the absorption of light by the free carriers [15]. Eventually, the threshold pumping intensity was determined as the value when the carrier density in the conduction band reaches 1×10^{19} cm^{-3} by the end of the pump pulse. The shaded bands in Fig. 4 depict the theoretically calculated pump threshold intensities, with (green) and without (purple) free-carrier absorption, for the experimentally used pulse durations of 80 (upper line) and 140 fs (lower line).

In our model, we use the Keldysh formalism and a Drude-like model to simulate the interband excitation and FCA processes. This allows us to investigate the role of the multiphoton and tunneling excitation process. Further, the combination of the Keldysh excitation and the Drude-like model has been successfully applied to understand laser-induced damages in solids where avalanche excitation upon the free-carrier absorption plays a key role as well [15].

While the measured wavelength dependence of the threshold pump intensity of ZnO thin films coincides qualitatively well with the simulated values taking FCA into account, the calculations without FCA deviate significantly. Thus, the initial increase of the threshold pump intensity between 1.2 and

2 μm can be understood in accordance with the multiphoton absorption picture of light. Increasing the laser wavelength (i.e., lowering the photon energy) leads to an increasing number of excitation photons needed to accommodate energy conservation and overcome the band gap. Comparison between the simulated threshold pump intensity with and without impact excitation suggests that there is no significant influence of FCA for pump wavelengths shorter than 1.2 μm.

The transition from a multiphoton to a tunneling-dominated carrier excitation process is expected at 2 μm (see the Supplemental Material [28]) using the Keldysh theory and a laser intensity of 0.5 TW/cm² [51]. In the tunneling regime, the excitation rate is weakly dependent on the laser wavelength compared to the multiphoton excitation regime. Therefore, we conclude that the threshold pump intensity decrease for longer wavelengths is caused by interband excitations via the field-driven electron impact.

A similar wavelength scaling of light absorption, also characterized by a pronounced minimum, was obtained in wide-band-gap dielectrics. In this way, the laser-induced damage threshold and the plasma formation threshold were used to monitor the excited electron density [15,21,52]. Our approach to use the onset of lasing is reversible and has the additional advantage that the observed threshold is very sharp and easy to detect in the experiment (see Fig. 2).

Simple quasiclassical calculations of electron motion in the ZnO conduction band, based on the solution of the equation for the quasimomentum in the presence of the laser field, show that for the threshold intensities determined in our experiments, the field strength is not high enough to accelerate electrons to energies exceeding the band-gap energy even for the longest 10 μm wavelength. Therefore, multiple scatterings are still required to heat electrons up to energies that are sufficient for the impact excitation. The best agreement between experimentally measured and theoretically determined values was achieved using an electron scattering time of $\sim$4 fs (see the Supplemental Material [28]). Our assumption of such a high frequency of the scattering processes is in agreement with previously reported electron scattering and dephasing times in strong-field experiments where the electrons are accelerated to high kinetic energies, as was the case in this work, too. In recently published works, the scattering-induced dephasing time of electrons driven by strong laser fields was in the range of a few femtoseconds (2–10 fs) [2,13,53–56]. Additionally, a comparison between the experimentally and theoretically determined peak-to-valley ratio of HHG spectra suggests a dephasing time of 4 fs for ZnO [9].

Since the simulations did not include the spot size dependence of the pump laser threshold intensity, no comparison of the absolute values obtained in the experiment and from theory is possible. However, our results demonstrate that lasing in semiconductors can be achieved with arbitrary pump wavelengths if the laser pulses are intense and short enough to initiate tunneling excitation and to avoid material damage as a consequence of an uncontrolled avalanche.

IV. CONCLUSION

The absorption of near- to far-infrared intense light in the wide-band-gap semiconductor ZnO was experimentally studied using the onset of stimulated emission (lasing) to probe the density of excited carriers. Stimulated emission was observed in a huge excitation energy range, where the ratio of the material band gap to the energy of absorbed photons spanned the range from 4 to 26. Toward longer wavelengths, the electron excitation mechanism changes from multiphoton absorption to tunneling, while an increasing role of electron impact excitation upon intraband free-carrier absorption was revealed. This leads to the remarkable result that the lowest threshold pump intensity to observe lasing emission was determined for the longest applied pump wavelength. The wavelength scaling of the lasing threshold intensity is in good agreement with calculations including multiphoton and tunneling excitation as well as free-carrier absorption. Manipulation of semiconductors with intense off-resonance light is possible in a broad spectral range and demonstrates the possibility of an easy integration of light-driven electronics in well-established platforms, such as those based on the telecom wavelengths (1.2–1.6 μm) [16].

Using ZnO allows us to perform experiments in an ambient atmosphere, and it enables an easy detection of NUV emission and far-off-resonance optical pumping in the spectral transparency regions of air. Although, as mentioned earlier, the process of off-resonant excitation is not restricted to semiconductors with band gaps in the NUV spectral rang. Hence, the possibility of UV lasing in hexagonal boron-nitride (hBN) at 215 nm (5.8 eV) upon electron beam excitation has been demonstrated previously [57]. Although to the best of our knowledge optically pumped stimulated emission from hBN is still missing, lasing from both ZnO (see Fig. 2) and hBN pumped optically and by accelerated electrons [57] is characterized by a rapid increase of the output signal and spectral narrowing when the lasing threshold pump intensity is reached. Thus, by using dielectrics with band gaps in the extreme ultraviolet (XUV) spectral range, excited by well-established ultrashort NIR pulses, our results suggest the possibility of an efficient optically pumped XUV source for the technologically important short-wavelength spectral range.

In the literature, an efficient HHG process in ZnO from laser wavelengths in the range between 1.8 and 4 μm was reported [58,59] when half the oscillation period of the electric field is around 3 and 7 fs, respectively. In this context, our findings will contribute to the discussion on the role of electron scattering processes in the HHG process.

All data needed to evaluate the conclusions made herein are present in the paper and/or the Supplemental Material [28]. Additional data related to this paper may be requested from the authors.

ACKNOWLEDGMENTS

R.H. and C.S. acknowledge financial support from the Helmholtz Institute Jena and from the German Research Society (DFG) via the International Research Training Group (IRTG) 2101. We also acknowledge the support via the CRC 1375 "NOA" funded by the DFG. M.Z. acknowledges support by the Max Planck Society (Max Planck Research Group) and the Federal Ministry of Education and Research (BMBF) under "Make our Planet Great Again–German Research

Initiative" (Grant No. 57427209 "QUESTforENERGY") implemented by DAAD. F.L. acknowledges support from the Canada Foundation for Innovation (CFI), the Natural Sciences and Engineering Research Council of Canada (NSERC)), the Fonds de Recherche du Québec sur la Nature et les Technologies (FRQNT), and the Ministère de l'Économie et de l'Innovation du Québec (MEI). E.H. acknowledges financial support from NSERC Ph.D. scholarship program. We thank Thomas Brabec for helpful discussion. Further, we thank Philippe Lassonde for his help characterizing the 10 μm laser pulses. We also want to acknowledge fruitful discussions with Stefanie Gräfe, Martin Richter, Christian Hünecke, Ivan Gonoskov, Ulf Peschel, Thomas Lettau, Silvana Botti, and Xiao Chen.

R.H., D.K., and C.S. conceived the idea. R.H. and P.H. conducted the experiments using a 3.2 μm laser. R.H. and V.S. conducted the experiments using a 3.75 μm laser. R.H. and E.H. conducted the experiments using a 10 μm laser. R.H. performed the wavelength scan and the simulations. U.R. fabricated the polycrystalline ZnO thin film sample. Maximilian Zapf performed the SEM characterization of the film. I.U. performed the XRD characterization of the film. R.H. wrote the manuscript with contributions from all other coauthors.

The authors declare that they have no competing interests.

[1] M. M. Waldrop, The chips are down for Moore's law, Nature **530**, 144 (2016).

[2] H. Mashiko, K. Oguri, T. Yamaguchi, A. Suda, and H. Gotoh, Petahertz optical drive with wide-bandgap semiconductor, Nat. Phys. **12**, 741 (2016).

[3] M. Schultze, E. Bothschafter, A. Sommer, S. Holzner, W. Schweinberger, M. Fiess, M. Hofstetter, R. Kienberger, V. Apalkov, V. S. Yakovlev, M. I. Stockman, and F. Krausz, Controlling dielectrics with the electric field of light, Nature **493**, 75 (2013).

[4] H. Mashiko, Y. Chisuga, I. Katayama, K. Oguri, H. Masuda, J. Takeda, and H. Gotoh, Multi-petahertz electron interference in Cr:Al2O3 solid-state material, Nat. Commun. **9**, 1468 (2018).

[5] J. Schoetz, Z. Wang, E. Pisanty, M. Lewenstein, M. F. Kling, and M. F. Ciappina, Perspective on petahertz electronics and attosecond nanoscopy, ACS Photon. **6**, 3057 (2019).

[6] F. Langer, C. P. Schmid, S. Schlauderer, M Gmitra, J. Fabian, P. Nagler, C. Schüller, T. Korn, P. G. Hawkins, J. T. Steiner, U. Huttner, S. W. Koch, M. Kira, and R. Huber, Lightwave valleytronics in a monolayer of tungsten diselenide, Nature **557**, 76 (2018).

[7] A. Schiffrin, T. Paasch-Colberg, N. Karpowicz, V. Apalkov, D. Gerster, S. Mühlbrandt, M. Korbman, J. Reichert, M. Schultze, S. Holzner, J. V. Barth, R. Kienberger, R. Ernstorfer, V. S. Yakovlev, M. I. Stockman, and F. Krausz, Optical-field-induced current in dielectrics, Nature **493**, 70 (2013).

[8] S. Ghimire and D. A. Reis, High-harmonic generation from solids, Nat. Phys. **15**, 10 (2019).

[9] G. Vampa, C. R. McDonald, G. Orlando, D. D. Klug, P. B. Corkum, and T. Brabec, Theoretical Analysis of High-Harmonic Generation in Solids, Phys. Rev. Lett. **113**, 073901 (2014).

[10] N. Tancogne-Dejean, O. D. Mücke, F. X. Kärtner, and A. Rubio, Impact of the Electronic Band Structure in High-Harmonic Generation Spectra of Solids, Phys. Rev. Lett. **118**, 087403 (2017).

[11] M. Garg, M. Zhan, T. Luu, T. Klostermann, A. Guggenmos, and E. Goulielmakis, Multi-petahertz electronic metrology, Nature **538**, 359 (2016).

[12] A. A. Lanin, E. A. Stepanov, A. V. Mitrofanov, D. A. Sidorov-Biryukov, A. B. Fedotov, and A. M. Zheltikov, High-order harmonic analysis of anisotropic petahertz photocurrents in solids, Opt. Lett. **44**, 1888 (2019).

[13] S. Y. Kruchinin, F. Krausz, and V. S. Yakovlev, Colloquium: Strong-field phenomena in periodic systems, Rev. Mod. Phys. **90**, 021002 (2018).

[14] H. Hirori, K. Shinokita, M. Shirai, S. Tani, Y. Kadoya, and K. Tanaka, Extraordinary carrier multiplication gated by a picosecond electric field pulse, Nat. Commun. **2**, 594 (2011).

[15] D. Ristau, *Laser-Induced Damage in Optical Materials* (Taylor & Francis, London, 2014).

[16] A. Wallucks, I. Marinković, B. Hensen, R. Stockill, and S. Gröblacher, A quantum memory at telecom wavelengths, Nat. Phys. **16**, 772 (2020).

[17] F. Schlaepfer, M. Lucchini, S. A. Sato, M. Volkov, L. Kasmi, N. Hartmann, A. Rubio, L. Gallmann, and U. Keller, Attosecond optical-field-enhanced carrier injection into the GaAs conduction band, Nat. Phys. **14**, 560 (2018).

[18] M. Kozák, M. Martínek, T. Otobe, F. Trojánek, and P. Malý, Observation of ultrafast impact ionization in diamond driven by mid-infrared femtosecond pulses, J. Appl. Phys. **128**, 015701 (2020).

[19] S. A. Sato, M. Lucchini, M. Volkov, F. Schlaepfer, L. Gallmann, U. Keller, and A. Rubio, Role of intraband transitions in photocarrier generation, Phys. Rev. B **98**, 035202 (2018).

[20] C. R. McDonald, A. Ben Taher, and T. Brabec, Strong optical field ionization of solids, J. Opt. **19**, 114005 (2017).

[21] E. Migal, E. Mareev, E. Smetanina, G. Duchateau, and F. Potemkin, Role of wavelength in photocarrier absorption and plasma formation threshold under excitation of dielectrics by high-intensity laser field tunable from visible to mid-IR, Sci. Rep. **10**, 14007 (2020).

[22] M. A. M. Versteegh, T. Kuis, H. T. C. Stoof, and J. I. Dijkhuis, Ultrafast screening and carrier dynamics in ZnO: Theory and experiment, Phys. Rev. B **84**, 035207 (2011).

[23] P. Zu, Z. K. Tang, G. K. L. Wong, M. Kawasaki, A. Ohtomo, H. Koinuma, and Y. Segawa, Ultraviolet spontaneous and stimulated emissions from ZnO microcrystallite thin films at room temperature, Solid State Commun. **103**, 459 (1997).

[24] R. Hollinger, D. Gupta, M. Zapf, M. Karst, R. Röder, I. Uschmann, U. Reislöhner, D. Kartashov, C. Ronning, and C. Spielmann, Polarization dependent multiphoton absorption in ZnO thin films, J. Phys. D **53**, 055102 (2019).

[25] Y. Huang, H. Zhu, H. Zheng, Z. Tang, J. Dong, S. Su, Y. Shen, X. Gui, S. Deng, and Z. Tang, Five-photon absorption upconversion lasing from on-chip whispering gallery mode, Nanoscale **12**, 6130 (2020).

[26] H. Zhu, A. Q. Chen, Y. Y. Wu, W. F. Zhang, S. C. Su, X. Ji, P. T. Jing, S. F. Yu, C. X. Shan, and F. Huang, Seven-photon-excited upconversion lasing at room temperature, Adv. Opt. Mat. **6**, 1800518 (2018).

[27] R. Hollinger, P. Malevich, V. Shumakova, S. Ališauskas, M. Zapf, R. Röder, A. Pugžlys, A. Baltuška, C. Ronning, C. Spielmann, and D. Kartashov, Strong light-field driven nanolasers, Nano Lett. **19**, 3563 (2019).

[28] See Supplemental Material at http://link.aps.org/supplemental/10.1103/PhysRevB.104.035203 for further information on the ZnO thin film characterization using SEM and XRD methods; an illustration of the experimental setups used to perform the spectrally and temporally resolved measurements; a measured high harmonic spectrum and the dependence of HHG on the mid-IR laser intensity; detailed information on the model used to simulate the optically pumped laser emission from ZnO; an illustration and discussion of the pump laser spot size dependent lasing threshold intensity; the measured polarization state of the near-ultraviolet emission around 390 nm below and above the threshold pump intensity; the spectral evolution of the near-ultraviolet emission spectra as a function of the pump laser intensity for 1.5, 2.4, 3.75, and 10 μm pump laser wavelengths; a schematic illustration of the multiphoton absorption and tunneling process; an illustration of the electron generation rate for a fixed laser intensity of 0.5 TW/cm², determined from the Keldysh model; an introduction of the Keldysh parameter, used to distinguish between the multiphoton and tunneling regime; a discussion on the electron scattering time in the applied model; a calculation of the threshold pump intensities for a set of electron scattering times; and verification of the best agreement between the calculated and measured threshold pump intensities for an electron scattering time of 4 fs. Including Refs. [29–39].

[29] E. Zolotoyabko, *Basic Concepts of X-Ray Diffraction* (Wiley, New York, 2014).

[30] S. Ghimire, A. D. DiChiara, E. Sistrunk, P. Agostini, L. F. DiMauro, and D. A. Reis, Observation of high-order harmonic generation in a bulk crystal, Nature Phys. **7**, 138 (2011).

[31] E. V. Chelnokov, N. Bityurin, I. Ozerov, and W. Marine, Two-photon pumped randomlaser in nanocrystalline ZnO, Appl. Phys. Lett. **89**, 171119 (2006).

[32] H. Cao, Y. G. Zhao, S. T. Ho, E. W. Seelig, Q. H. Wang, and R. P. H. Chang, Randomlaser Action in Semiconductor Powder, Phys. Rev. Lett. **82**, 2278 (1999).

[33] H. Cao, J. Y. Xu, S.-H. Chang, and S. T. Ho, Transition from amplified spontaneous emission to laser action in strongly scattering media, Phys. Rev. E **61**, 1985 (2000).

[34] G. P. Agrawal and N. K. Dutta, *Semiconductor Lasers* (Springer Science & Business Media, Berlin, 2013).

[35] Z. K. Tang, M. Kawasaki, A. Ohtomo, H. Koinuma, and Y. Segawa, Self-assembled ZnO nano-crystals and exciton lasing at room temperature, J. Cryst. Growth **287**, 169 (2006).

[36] P. C. Becker, H. L. Fragnito, C. H. Brito Cruz, R. L. Fork, J. E. Cunningham, J. E. Henry, and C. V. Shank, Femtosecond Photon Echoes from Band-to-Band Transitions in GaAs, Phys. Rev. Lett. **61**, 1647 (1988).

[37] M. T. Portella, J.-Y. Bigot, R. W. Schoenlein, J. E. Cunningham, and C. V. Shank, k-space carrier dynamics in GaAs, Appl. Phys. Lett. **60**, 2123 (1992).

[38] B. B. Hu, E. A. de Souza, W. H. Knox, J. E. Cunningham, M. C. Nuss, A. V. Kuznetsov, and S. L. Chuang, Identifying the Distinct Phases of Carrier Transport in Semiconductors with 10 fs Resolution, Phys. Rev. Lett. **74**, 1689 (1995).

[39] J. L. Oudar, D. Hulin, A. Migus, A. Antonetti, and F. Alexandre, Subpicosecond Spectral Hole Burning Due to Nonthermalized Photoexcited Carriers in GaAs, Phys. Rev. Lett. **55**, 2074 (1985).

[40] N. C. Geib, R. Hollinger, E. Haddad, P. Herrmann, F. Légaré, T. Pertsch, C. Spielmann, M. Zürch, and F. Eilenberger, Discrete dispersion scan setup for measuring few-cycle laser pulses in the mid-infrared, Opt. Lett. **45**, 5295 (2020).

[41] J. Shah, *Ultrafast Spectroscopy of Semiconductors and Semiconductor Nanostructures* (Springer Science & Business Media, Berlin, 1999).

[42] M. Kawasaki, A. Ohtomo, I. Ohkubo, H. Koinuma, Z. K. Tang, P. Yu, G. K. L. Wong, B. P. Zhang, and Y. Segawa, Excitonic ultraviolet laser emission at room temperature from naturally made cavity in ZnO nanocrytal thin films, Mater. Sci. Eng.: B **56**, 239 (1998).

[43] R. Hollinger, P. Herrmann, V. Korolev, M. Zapf, V. Shumakova, R. Röder, I. Uschmann, A. Pugžlys, A. Baltuška, M. Zürch, C. Ronning, C. Spielmann, and D. Kartashov, Polarization dependent excitation and high harmonic generation from intense mid-IR laser pulses in ZnO, Nanomaterials **11**, 4 (2021).

[44] M. Wille, C. Sturm, T. Michalsky, R. Röder, C. Ronning, R. Schmidt-Grund, and M. Grundmann, Carrier density driven lasing dynamics in ZnO nanowires, Nanotechnology **32**, 225702 (2016).

[45] L. Bergman, X.-B. Chen, J. L. Morrison, J. Huso, and A. P. Purdy, Photoluminescence dynamics in ensembles of wide-band-gap nanocrystallites and powders, J. Appl. Phys. **96**, 675 (2004).

[46] Y. Yang, H. Yan, Z. Fu, B. Yang, L. Xia, Y. Xu, J. Zuo, and F. Li, Photoluminescence investigation based on laser heating effect in ZnO-ordered nanostructures, J. Phys. Chem. B **110**, 846 (2006).

[47] C. F. Klingshirn, *Semiconductor Optics* (Springer Science & Business Media, Berlin, 2012).

[48] J. C. Johnson, K. P. Knutsen, H. Yan, M. Law, Y. Zhang, P. Yang, and R. J. Saykally, Ultrafast carrier dynamics in single ZnO nanowire and nanoribbon lasers, Nano Lett. **4**, 197 (2004).

[49] R. Röder and C. Ronning, Review on the dynamics of semiconductor nanowire lasers, Semicond. Sci. Technol. **33**, 033001 (2018).

[50] S. Richter, O. Herrfurth, S. Espinoza, M. Rebarz, M. Kloz, J. A. Leveillee, A. Schleife, S. Zollner, M. Grundmann, J. Andreasson, and R. Schmidt-Grund, Ultrafast dynamics of hot charge carriers in an oxide semiconductor probed by femtosecond spectroscopic ellipsometry, New J. Phys. **22**, 083066 (2020).

[51] L. V. Keldysh, Ionization in the field of a strong electromagnetic wave, Sov. Phys. JETP **20**, 1307 (1965).

[52] D. M. Simanovskii, H. A. Schwettman, H. Lee, and A. J. Welch, Mid-Infrared Optical Breakdown in Transparent Dielectrics, Phys. Rev. Lett. **91**, 107601 (2003).

[53] A. Pati, I. Wahyutama, and A. Pfeiffer, Subcycle-resolved probe retardation in strong-field pumped dielectrics, Nat. Commun. **6**, 7746 (2015).

[54] I. Floss, Ch. Lemell, G. Wachter, V. Smejkal, S. A. Sato, X.-M. Tong, K. Yabana, and J. Burgdörfer, *Ab initio* multiscale simulation of high-order harmonic generation in solids, Phys. Rev. A **97**, 011401(R) (2018).

[55] A. N. Pfeiffer, Iteration of semiconductor Bloch equations for ultrashort laser pulse propagation, J. Phys. B **53**, 164002 (2020).

[56] R. Géneaux, C. J. Kaplan, L. Yue, A. D. Ross, J. E. Bækhøj, P. M. Kraus, H.-T. Chang, A. Guggenmos, M.-Y. Huang, M. Zürch, K. J. Schafer, D. M. Neumark, M. B. Gaarde, and S. R. Leone, Attosecond Time-Domain Measurement of Core-Level-Exciton Decay in Magnesium Oxide, Phys. Rev. Lett. **124**, 207401 (2020).

[57] K. Watanabe, T. Taniguchi, and H. Kanda, Direct-bandgap properties and evidence for ultraviolet lasing of hexagonal boron nitride single crystal, Nat. Mater. **3**, 404 (2004).

[58] Z. Wang, H. Park, Y. H. Lai, J. Xu, I. C. Blaga, F. Yang, P. Agostini, and L. F. DiMauro, The roles of photo-carrier doping and driving wavelength in high harmonic generation from a semiconductor, Nat. Commun. **8**, 1686 (2017).

[59] S. Gholam-Mirzaei, J. Beetar, and M. Chini, High harmonic generation in ZnO with a high-power mid-IR OPA, Appl. Phys. Lett. **110**, 061101 (2017).